Ann Nucl Med (2013) 27:847–854
DOI 10.1007/s12149-013-0757-x

ORIGINAL ARTICLE

Feasibility and kinetic characteristics of ^{68}Ga-NOTA-RGD PET for in vivo atherosclerosis imaging

Jin Chul Paeng · Yun-Sang Lee · Jae Sung Lee · Jae Min Jeong · Ki-Bong Kim · June-Key Chung · Dong Soo Lee

Received: 22 April 2013 / Accepted: 9 July 2013 / Published online: 6 August 2013

Abstract
Objective In this study, the feasibility and kinetic characteristics of the ^{68}Ga-NOTA-RGD, a recently developed RGD peptide agent, were investigated for atherosclerosis imaging in comparison with ^{18}FDG.
Methods ApoE$^{-/-}$ mice were fed a high-fat diet for more than 20 weeks. To evaluate the feasibility, tissue uptakes of ^{68}Ga-NOTA-RGD and ^{18}FDG in the major organs were measured and compared between ApoE$^{-/-}$ and control mice. Animal PET imaging was also performed and relative uptake values in the thoracic aorta were compared between ApoE$^{-/-}$ and control mice. In humans, the kinetic characteristics and feasibility of ^{68}Ga-NOTA-RGD PET were assessed in 4 patients with known coronary artery disease.
Results In the tissue uptake study, the thoracic aorta showed higher uptake in ApoE$^{-/-}$ than in control mice with both ^{68}Ga-NOTA-RGD and ^{18}FDG ($P < 0.001$). On PET scans, the relative uptake values of the thoracic aorta were significantly higher in ApoE$^{-/-}$ with both ^{68}Ga-NOTA-RGD ($P = 0.024$) and ^{18}FDG ($P = 0.038$). In human PET, the appropriateness of reversible binding model and Logan plotting was clearly demonstrated. The aorta-to-jugular ratios were measured up to 1.25 and showed a tendency to correlate with the serum high-sensitivity C-reactive protein level ($r = 0.899$, $P = 0.102$).
Conclusions ^{68}Ga-NOTA-RGD has potential as an in vivo atherosclerosis imaging agent. However, the lower imaging contrast and sensitivity of ^{68}Ga-NOTA-RGD PET compared with ^{18}FDG PET may be a limitation for clinical application.

Keywords Atherosclerosis · Vulnerable plaque · Molecular imaging · ^{68}Ga-NOTA-RGD · PET

J. C. Paeng · Y.-S. Lee · J. S. Lee · J. M. Jeong · J.-K. Chung · D. S. Lee (✉)
Department of Nuclear Medicine, Seoul National University College of Medicine, 101 Daehak-ro, Jongno-gu, Seoul 110-744, Korea
e-mail: dsl@snu.ac.kr

J. C. Paeng
e-mail: paengjc@snu.ac.kr

K.-B. Kim
Department of Thoracic and Cardiovascular Surgery, Seoul National University College of Medicine, Seoul, Korea

D. S. Lee
Department of Molecular Medicine and Biopharmaceutical Sciences, Seoul National University, Seoul, Korea

Introduction

Coronary and cerebrovascular diseases resulting from atherosclerosis are usually included among the three most common causes of death in worldwide surveys. Atherosclerotic plaques with vascular narrowing can be morphologically visualized by conventional coronary angiography (CAG), computed tomography (CT), and magnetic resonance imaging (MRI); however, the simple presence of atherosclerosis or vascular narrowing has limited clinical significance. In fact, in a considerable proportion of myocardial infarcts, the culprit coronary lesions do not show critical narrowing [1]. Additionally, in up to 62 % of male and 42 % of female patients, the first manifestation of coronary disease is a fatal myocardial infarct or sudden death without preceding ischemic symptoms [2]. Therefore, atherosclerotic plaque that carries high risk of fatal complications should be discriminated from simple plaque.

To image vulnerable plaques, various molecular imaging methods and targets have been utilized [3].

Inflammation is an excellent imaging target that can be easily imaged by 2-deoxy-2-[^{18}F]fluoro-D-glucose (^{18}FDG), the most widely used positron emission tomography (PET) imaging agent. ^{18}FDG PET has proven to be effective for the imaging of atherosclerosis in numerous clinical studies [4–8]; however, as ^{18}FDG is a non-specific tracer for glucose metabolism, other non-specific inflammation may be visualized on ^{18}FDG PET. Additionally, the myocardium, which is a critical site of insult in atherosclerosis, may show physiologically variable ^{18}FDG uptake. Thus, alternative atherosclerosis imaging methods are required, particularly when the coronary arteries are imaging targets.

Enhanced expression of integrin αvβ3 has been reported as another target mechanism of atherosclerosis. In vulnerable plaque, integrin expression is enhanced at the surface of activated angiogenic endothelial cells and macrophages. Currently, an excellent targeting moiety for integrin αvβ3 is available: the tri-peptide Arg–Gly–Asp (RGD), a component of fibronectin or vitronectin, has strong affinity for integrin αvβ3. Several RGD-containing imaging probes have been used as vulnerable plaque imaging agents for MRI or optical imaging [9, 10]. An RGD-based nuclear imaging method using [^{18}F]galacto-RGD was also tried in a mouse model, in which atherosclerotic plaques demonstrated greater uptake than normal vessel walls on animal PET [11].

Recently, we developed a ^{68}Ga-labeled RGD agent based on 1,4,7-triazacyclononane-1,4,7-triacetic acid (NOTA) [12]. ^{68}Ga-NOTA-RGD is a conjugate of c(RGDyK) and 2-(*p*-isothiocyanatobenzyl)-NOTA (SCN-Bn-NOTA). ^{68}Ga has a half-life of 68 min and emits 600 keV positrons. As ^{68}Ga is produced from a ^{68}Ge/^{68}Ga generator, it has good accessibility and can be inexpensive. ^{68}Ga-NOTA-RGD was successfully used to image angiogenic activity of tumors; thus, it is expected to be useful for atherosclerosis imaging.

In this study, the feasibility and imaging characteristics of ^{68}Ga-NOTA-RGD were investigated in comparison with ^{18}FDG using an animal model to evaluate its potential as an in vivo atherosclerosis imaging agent. Additionally, the kinetic characteristics and imaging feasibility in humans were investigated.

Materials and methods

Preparation of ^{68}Ga-NOTA-RGD

^{68}Ga-NOTA-RGD was prepared as previously described [12]. In brief, SCN-Bn-NOTA and c(RGDyK) were purchased from Futurechem (Seoul, Korea). They were mixed and allowed to react with each other for 20 h in 0.1 M Na_2CO_3 solution at room temperature and the reaction mixture was purified by high-performance liquid chromatography (HPLC; XTerra preparative column RP18, 10 × 250 mm, 0–100 % ethanol gradient in 0.01 % trifluoroacetic acid from 0 to 30 min, 3 mL/min of flow rate) for NOTA-RGD to be collected. ^{68}Ga (740 MBq in 1 mL of 0.1 N HCl) was eluted from a ^{68}Ge/^{68}Ga generator (Eckert & Ziegler, Berlin, Germany) and added to the NOTA-RGD solution (30 nmol in 0.1 mL of water). After 10 min incubation at room temperature, ^{68}Ga-NOTA-RGD was purified by HPLC (with the same condition as described above) and Alumina N Sep-Pak® cartridge to remove ^{68}Ge and free ^{68}Ga.

Animal model

As a mouse model of atherosclerosis, apolipoprotein E (ApoE)$^{-/-}$ B6 mice were obtained from the Center for Animal Resource Development at Seoul National University. After the age of 8 weeks, ApoE$^{-/-}$ mice were fed a high-fat Western diet containing 21.2 % total fat, 0.2 % cholesterol, 17.3 % protein, and 48.5 % carbohydrate (Feedlab, Seongnam, Korea). After more than 20 weeks on the high-fat Western diet, the mice were used for a tissue uptake study and PET imaging. Wild-type ICR mice were used as a control group. All animal experiments were approved by the Institutional Animal Care and Use Committee of Seoul National University Hospital.

Tissue uptake study

Tissue uptake in the major organs (heart, lung, liver, and descending thoracic aorta) was measured for ^{68}Ga-NOTA-RGD and ^{18}FDG. ApoE$^{-/-}$ ($n = 3$) and control ICR mice ($n = 3$) were injected with ^{68}Ga-NOTA-RGD (370 kBq/0.1 mL) via the tail vein. The mice were sacrificed by cervical dislocation 30 min after injection. The aorta and major organs were immediately obtained and weighed. The radioactivity of each organ was measured using a gamma counter (Cobra II, Packard Canberra Co., USA). Tissue uptake in each organ is expressed as %ID/g. To analyze ^{18}FDG tissue uptake, other groups of ApoE$^{-/-}$ ($n = 3$) and control mice ($n = 3$) were fasted for more than 12 h, and ^{18}FDG (74 kBq/0.1 mL; synthesized in-house cyclotron and commercial modules, FASTlab, GE Healthcare, USA) was injected via the tail vein. The mice were sacrificed 45 min after injection, and tissue radioactivity in the aorta and major organs was measured by the same method described above.

^{68}Ga-NOTA-RGD PET in mice

Dynamic PET for ^{68}Ga-NOTA-RGD was performed to establish an imaging protocol. ApoE$^{-/-}$ mice ($n = 3$) were anesthetized with 2 % isoflurane, and ^{68}Ga-NOTA-RGD was injected via the tail vein (18.5 MBq/0.1 mL). Immediately after injection, a dynamic PET scan was performed for 60 min with the list mode using a dedicated small animal PET/CT scanner (eXplore Vista, GE Healthcare, USA). A dynamic PET scan was performed for one bed position covering a 4.6 cm field of view (FOV) from the upper neck to the bladder. After PET acquisition, a CT scan was performed for the same FOV. The acquired images were framed into 12 × 5 min frame images and reconstructed by a 3-D ordered subset expectation maximization (OSEM) algorithm method with 16 iterations, combined with scatter and random corrections. The reconstructed PET images were displayed as transaxial images fused with the CT images. Volumes of interest (VOIs) were drawn for the descending thoracic aorta (covering from the end of aortic arch to the diaphragm level), lungs, heart, and liver, using an open-source software package (OsiriX, available at http://www.osirix-viewer.com). The mean uptake in each VOI was measured and expressed as the relative uptake value with the lungs set as a reference organ, because the lungs are the anatomical background of the aorta and normally show only low integrin expression and RGD uptake.

A ^{68}Ga-NOTA-RGD static PET scan was performed in ApoE$^{-/-}$ ($n = 7$) and control mice ($n = 4$) to evaluate the feasibility of using ^{68}Ga-NOTA-RGD PET for atherosclerosis imaging. The protocol for the static PET/CT scan was established based on the results of our ^{68}Ga-NOTA-RGD dynamic PET scans (see "Results"). Static PET was started 30 min after the injection of ^{68}Ga-NOTA-RGD (18.5 MBq) via the tail vein; a static PET image was acquired for 30 min. The bed position for image acquisition was the same as for the dynamic scan, with one bed position covering from the upper neck to the bladder. CT was performed before or after PET. A static PET scan was also reconstructed using the 3-D OSEM algorithm with scatter and random corrections. ^{18}FDG PET was also performed in ApoE$^{-/-}$ ($n = 6$) and control mice ($n = 4$). Forty minutes after the injection of ^{18}FDG (18.5 MBq) via the tail vein, the mice were subjected to static PET for 30 min. The image acquisition and reconstruction methods were the same as those used for ^{68}Ga-NOTA-RGD static PET. VOIs were also drawn for the major organs in both ^{68}Ga-NOTA-RGD and ^{18}FDG PET.

^{68}Ga-NOTA-RGD PET in humans

To assess the kinetic characteristics and feasibility of ^{68}Ga-NOTA-RGD PET in humans, four patients diagnosed with coronary artery disease were enrolled (all males, age range 37–79 years). The human PET studies were approved by our Institutional Review Board. After the injection of 180 MBq of ^{68}Ga-NOTA-RGD, a list-mode dynamic PET scan was performed for 60 min with the center of FOV placed on the heart using a PET/CT scanner (Biograph 40, Siemens, Germany).

Dynamic images were reconstructed into 27-frame images (6 × 10, 4 × 15, 4 × 30, 3 × 60, 4 × 120, 3 × 300, and 3 × 600 s). On fused images of dynamic PET and CT, VOIs were drawn for the left ventricle, descending thoracic aorta, liver, and paraspinal back muscle using a vendor-supplied software package (TrueD, Siemens Healthcare, Germany), and afterward, the mean radioactivity in each VOI was measured. A time–activity curve (TAC) for each organ was acquired from the measurements and used for kinetic analysis. Logan plotting, which is related with a three-compartment model, was adopted and the plotting equation was used as below.

$\mathrm{DVR} = \frac{\mathrm{DV_{target}}}{\mathrm{DV_{reference}}}$, where DV is the volume of distribution

$\mathrm{BP} = \mathrm{DVR} - 1$, where BP is the binding potential

The appropriateness of this approach was tested using the liver as a positive organ and muscle as a reference organ, according to previous reports on the kinetic characteristics of an ^{18}F-labeled RGD agent and integrin expression in the liver [13, 14].

For the physiological characterization of ^{68}Ga-NOTA-RGD PET imaging, static images were reconstructed using 30–60 min dynamic images. VOIs of the aorta were drawn to cover >3 cm of the descending thoracic aorta (from the end of aortic arch), using a vendor-supplied software package (TrueD, Siemens Healthcare, Germany). VOIs for the jugular vein were also drawn for normalization of the aortic uptake. The aorta-to-jugular ratio was calculated for each patient and compared with the radiologic findings for the aorta and laboratory finding of serum high-sensitivity C-reactive protein (hsCRP).

Statistics

All the quantitative data were expressed as mean ± SD. For comparison of uptake ratios between groups, Mann–Whitney rank sum tests were used and P values <0.05 were regarded as significant. A commercial software package (MedCalc 9.5.0.0, MedCalc Software, Mariakerke, Belgium) was used for all the statistical analyses.

Results

Preparation of ^{68}Ga-NOTA-RGD and animal model

Successful preparation and high labeling efficiency of ^{68}Ga-NOTA-RGD were confirmed by instant thin-layer

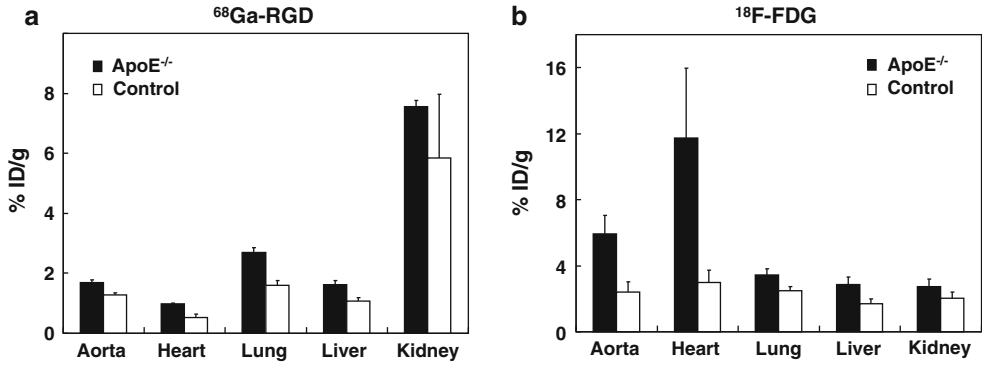

Fig. 1 Tissue uptake characteristics of ^{68}Ga-NOTA-RGD (**a**) and ^{18}FDG (**b**) in ApoE$^{-/-}$ and control mice. Although uptake in the thoracic aorta was higher in ApoE$^{-/-}$ mice both for ^{68}Ga-NOTA-RGD ($P < 0.001$) and ^{18}F-FDG ($P < 0.001$), the difference was much clearer with ^{18}F-FDG. Uptake in the heart was relatively higher with ^{18}F-FDG

chromatography-silica gel (ITLC-SG) in every synthesis and experiment. In ApoE$^{-/-}$ mice, the formation of atherosclerotic plaques after more than 20 weeks of high-fat Western diet was confirmed by histopathologic examination of the thoracic aorta.

Tissue uptake study

Uptake in the thoracic aorta was higher in ApoE$^{-/-}$ mice than in control mice for both ^{68}Ga-NOTA-RGD and ^{18}FDG (1.68 ± 0.11 vs. 1.28 ± 0.08 %ID/g for ^{68}Ga-NOTA-RGD, $P < 0.001$; and 5.91 ± 1.14 vs. 2.40 ± 0.65 %ID/g for ^{18}FDG, $P < 0.001$). However, the difference between the ApoE$^{-/-}$ and control mice was more marked with ^{18}FDG than with ^{68}Ga-NOTA-RGD (Fig. 1). Notably, however, the uptake in the heart was different between the two imaging agents; with ^{68}Ga-NOTA-RGD, the thoracic aorta showed greater uptake than the heart in both ApoE$^{-/-}$ and control mice, whereas the heart showed much greater and more variable uptake than the thoracic aorta in both the ApoE$^{-/-}$ and control mouse groups with ^{18}FDG (Fig. 1).

^{68}Ga-NOTA-RGD PET in mice

On ^{68}Ga-NOTA-RGD dynamic PET, the uptake in the aorta and major organs was measured and normalized to the initial lung uptake. The aorta showed greater uptake than the heart and lungs (Fig. 2). The lung uptake decreased gradually during the first 30 min and reached a plateau thereafter; the heart showed a more rapid decrease than the lungs during the first 30 min, and it decreased more slowly from around 30 min, demonstrating initial blood pool activity. Similarly, the aorta uptake also decreased rapidly during the initial 30 min and reached a slower decrease at around 30 min. According to our dynamic PET results, a protocol for ^{68}Ga-NOTA-RGD static PET was established as a 30 min static scan starting 30 min after injection of ^{68}Ga-NOTA-RGD.

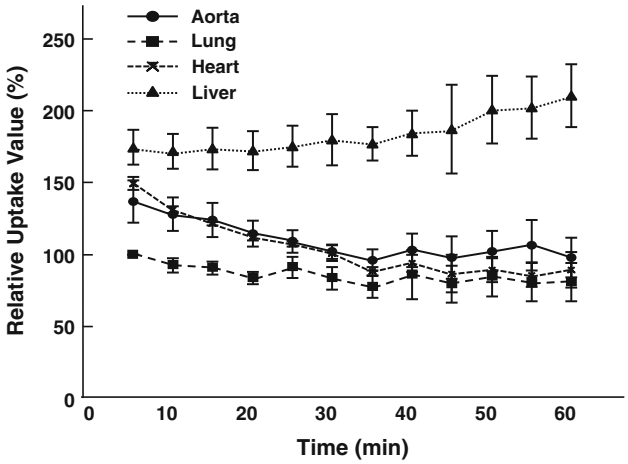

Fig. 2 Time–activity curves of the thoracic aorta and major organs in ApoE$^{-/-}$ mice on ^{68}Ga-NOTA-RGD dynamic PET. The thoracic aorta, heart, and lungs showed rapid decreases during the first 30 min followed by a plateau or slower decrease at about 30 min, probably due to blood pool activity. In contrast, the liver showed a gradual increase in uptake

On ^{68}Ga-NOTA-RGD and ^{18}FDG static PET, the relative uptake value of the thoracic aorta was significantly higher in the ApoE$^{-/-}$ than in the control mice for both ^{68}Ga-NOTA-RGD ($P = 0.024$) and ^{18}FDG ($P = 0.038$) (Table 1). Although the difference in uptake in the aorta between the ApoE$^{-/-}$ and control mice was more marked with ^{18}FDG, uptake in the heart was much lower and less variable with ^{68}Ga-NOTA-RGD than with ^{18}FDG in both the ApoE$^{-/-}$ and control mouse groups (Table 1). Typical ^{68}Ga-NOTA-RGD and ^{18}FDG PET images are shown in Fig. 3.

Kinetics and feasibility study in humans

In all patients, a good correlation was obtained by Logan plotting for the liver and muscle TACs after a moderate equilibrium

Table 1 Relative uptake values of the major organs on ^{68}Ga-NOTA-RGD and ^{18}FDG PET images of ApoE$^{-/-}$ and control mice

	ApoE$^{-/-}$	Control	*P*
^{68}Ga-NOTA-RGD	($n = 7$)	($n = 4$)	
Aorta	1.37 ± 0.11	1.20 ± 0.06	0.024
Heart	1.27 ± 0.15	1.14 ± 0.19	n. s.
Liver	2.48 ± 0.39	1.83 ± 0.18	0.006
	ApoE$^{-/-}$	Control	*P*
^{18}FDG	($n = 6$)	($n = 4$)	
Aorta	2.25 ± 1.05	1.23 ± 0.22	0.038
Heart	12.24 ± 8.20	8.32 ± 8.72	n. s.
Liver	1.27 ± 0.5	1.11 ± 0.18	n. s.

Organ-to-lung uptake ratio

time (20 min after injection), indicating the appropriateness of the application of the reversible binding model and Logan plotting to ^{68}Ga-NOTA-RGD PET data (Fig. 4). Based on the plotting, DV and BP were calculated for the livers and muscles of the patients, which were robust and showed little variation (Table 2). The results of static PET studies are summarized in Table 3 and a representative case is presented in Fig. 5. The aorta-to-jugular ratio was 1.07 ± 0.14 (range 0.93–1.25), whereas the serum hsCRP level was 2.65 ± 2.53 mg/L (range 0.6–6.3), which showed a tendency of correlation between the aorta-to-jugular ratio and hsCRP, although it was not statistically significant ($r = 0.899$, $P = 0.102$).

Discussion

In the present study, the feasibility and imaging characteristics of ^{68}Ga-NOTA-RGD for in vivo atherosclerosis imaging were investigated in an animal model and in humans. Our results demonstrate the potential of ^{68}Ga-NOTA-RGD as an imaging agent for atherosclerosis and the appropriateness of the reversible binding model and Logan plotting for human ^{68}Ga-NOTA-RGD PET. In human PET studies, ^{68}Ga-NOTA-RGD uptake showed a tendency to correlate with a clinical inflammation marker, serum hsCRP, in patients with mild aortic atherosclerosis.

As fatal events from atherosclerosis result from a rupture of plaques in critical arteries, the detection and evaluation of rupture-prone vulnerable plaques are valuable for direct risk assessment and treatment-target selection. For the molecular imaging of atherosclerosis, many pathophysiologic mechanisms and markers have been suggested [3, 15]. Among these, inflammation is the most widely studied because it plays a key role in the development of atherosclerosis at all stages, including initiation, progression, and rupture. With regard to inflammation, ^{18}FDG PET has been most widely studied because ^{18}FDG is easily accessible and very sensitive to inflammation. ^{18}FDG uptake in atherosclerosis has been correlated with activated macrophages [16, 17], inflammatory biomarkers [18, 19], plaque disruption [16], and prognosis [20]. Thus, ^{68}Ga-NOTA-RGD PET was compared with ^{18}FDG PET in the present study.

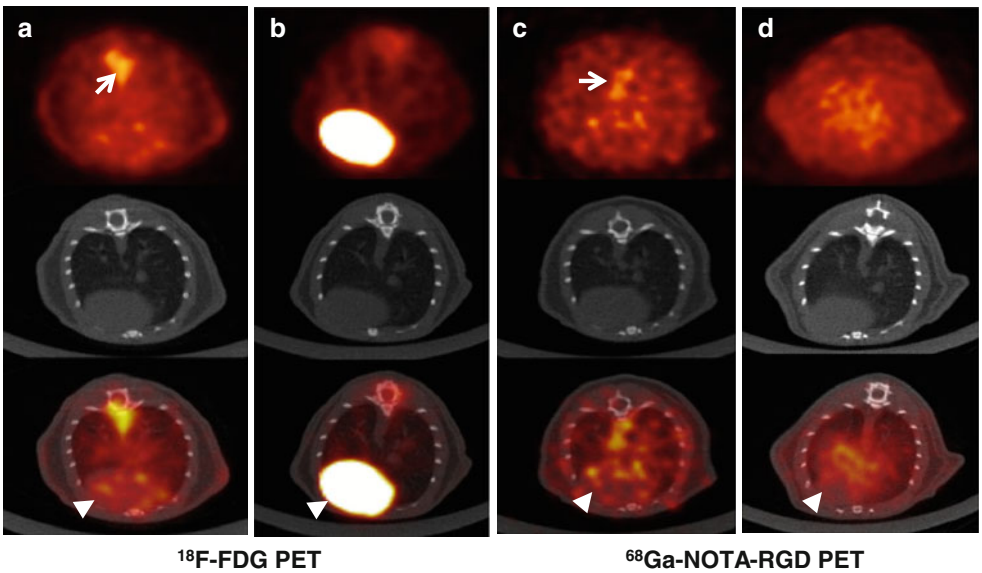

Fig. 3 ^{18}FDG PET (**a**, **b**) and ^{68}Ga-NOTA-RGD (**c**, **d**) images of ApoE$^{-/-}$ (**a**, **c**) and control (**b**, **d**) mice (*upper row* is PET, *middle row* CT, and *lower row* PET/CT fusion images). Increased uptake was observed in the thoracic aorta of ApoE$^{-/-}$ mice compared with those of controls (*arrow*). Although uptake in the aorta was clearer on ^{18}FDG PET, uptakes in the heart (*arrowhead*) and muscle were much more variable on ^{18}FDG PET compared with ^{68}Ga-NOTA-RGD PET. Here, the assignments of *middle* and *lower rows* were reversed, i.e. the *middle row* corresponds to the CT images and the *lower row* corresponds to the PET/CT fusion

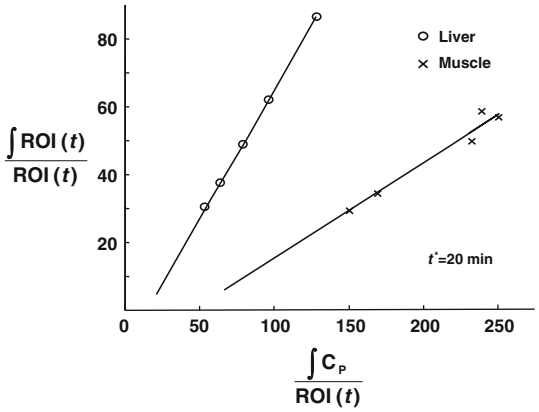

Fig. 4 Graphical analysis of a human ^{68}Ga-NOTA-RGD dynamic PET case using Logan plotting. The near-perfect linear regression 20 min after injection demonstrates the appropriateness of the reversible binding model and *Logan plotting*

Table 2 Distribution volumes and binding potentials calculated on human ^{68}Ga-NOTA-RGD dynamic PET

	Patient 1	Patient 2	Patient 3	Patient 4	Mean
DV of liver	0.97	0.73	0.77	0.75	0.80 ± 0.10
DV of muscle	0.35	0.25	0.23	0.29	0.28 ± 0.04
DV ratio	2.80	2.87	3.37	2.62	2.92 ± 0.28
Binding potential	1.80	1.87	2.37	1.62	1.92 ± 0.28

DV distribution volume

Integrin αvβ3 is highly expressed in activated endothelia; therefore, it is usually a target for angiogenesis imaging. In atherosclerosis, angiogenesis occurs in plaques when organized plaques become inflamed and prone to rupture [3, 21]. Additionally, activated macrophages strongly express integrin αvβ3 on their surface, which may be another imaging target, probably more significant than endothelia in murine models [22]. RGD agents have been developed for MRI and as optical imaging agents of atherosclerosis [9, 10]. In an optical imaging study using a cyanine 5.5-labeled RGD peptide, the carotid plaque showed strong fluorescence contrast, although it was detected in surgically opened tissue [10]. In an MRI study using a gadolinium (Gd)-conjugated RGD peptide, significant contrast enhancement was observed in carotid plaque [9].

[^{18}F]galacto-RGD was the first radiolabeled RGD agent used for the in vivo cardiologic imaging of atherosclerotic inflammation [11] and myocardial infarcts [23]. In a study of [^{18}F]galacto-RGD for atherosclerosis imaging, autoradiography and animal PET were performed for the quantitative assessment of plaque uptake, and the plaques demonstrated an increase in [^{18}F]galacto-RGD uptake of 1.4 times compared with normal vessels [11]. Another RGD agent, ^{68}Ga-DOTA-RGD, was assessed in an animal model using autoradiography; the plaque demonstrated 1.39 times greater uptake than the vessel wall [24]. Recently, we developed a novel radiolabeled RGD agent, ^{68}Ga-NOTA-RGD, which was successfully used to image hypervascular tumors in animals [12]. The present study demonstrated the efficacy of ^{68}Ga-NOTA-RGD as an atherosclerosis imaging agent in addition to tumor imaging.

In our tissue uptake study, the atherosclerotic aortas of ApoE$^{-/-}$ mice showed greater ^{68}Ga-NOTA-RGD uptake compared with those of control mice. Greater uptake in atherosclerotic aortas was also observed with ^{18}FDG, as expected. Based on this result, ^{68}Ga-NOTA-RGD PET was investigated after dynamic PET studies to establish an imaging protocol for ^{68}Ga-NOTA-RGD PET. In the dynamic study, the TACs of the aorta, lungs and heart demonstrated a rapid decrease during the initial phase, followed by a plateau or slower decrease after 30 min, reflecting the initial blood pool compartment. In contrast, the liver showed a gradual increase until the end of the scan, reflecting innate integrin expression [22].

On static PET, significantly greater uptake was observed in atherosclerotic aorta compared with the control with both ^{68}Ga-NOTA-RGD and ^{18}FDG PET. However, the difference between the atherosclerotic and control aorta was clearer with ^{18}FDG PET. The atherosclerotic aortas exhibited 1.15 times greater uptake than the controls with ^{68}Ga-NOTA-RGD PET, whereas 1.83 times greater uptake was observed with ^{18}FDG PET. Thus, the sensitivity of ^{68}Ga-NOTA-RGD PET is expected to be lower than that of ^{18}FDG PET. However, the low uptake detected in the heart and soft tissue might be an advantage of ^{68}Ga-NOTA-RGD compared with ^{18}FDG, as variable myocardial uptake is

Table 3 The aorta-to-jugular vein ratio on ^{68}Ga-NOTA-RGD PET in coronary artery disease patients with regard to their radiological and laboratory findings

	Patient 1	Patient 2	Patient 3	Patient 4
Aorta-to-jugular ratio	1.01	1.25	0.93	1.11
CTA	Calcified atheroma	Mild atherosclerosis	Mild atherosclerosis	Mild atherosclerosis
hsCRP (mg/L)	0.6	6.3	1.4	2.3

CTA computed tomography angiography finding of the aorta, *hsCRP* high-sensitivity C-reactive protein

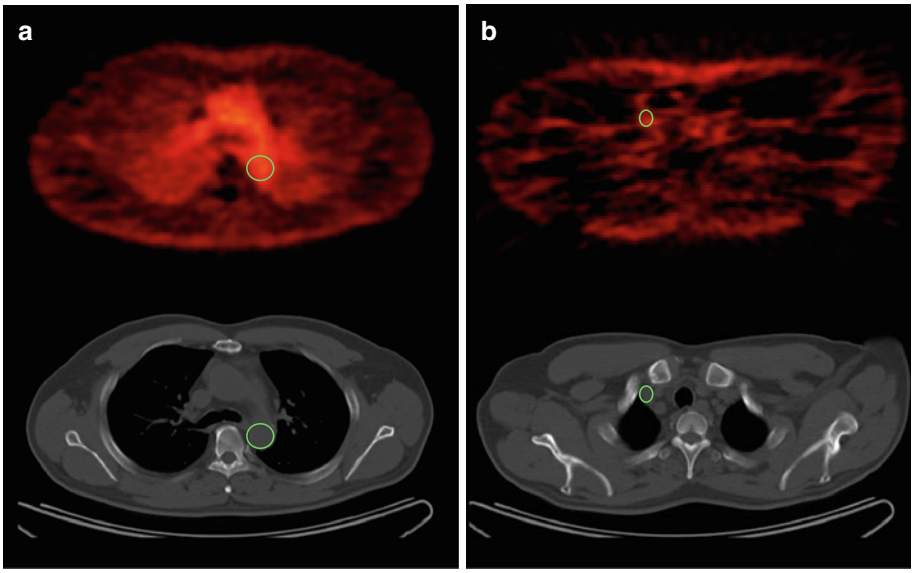

Fig. 5 A representative case of human ^{68}Ga-NOTA-RGD PET. Cylindrical VOIs were drawn for the aorta (**a**) and the jugular vein (**b**), respectively. The aorta-to-jugular ratio of this patient was calculated as 1.25

also frequently observed in human ^{18}FDG PET, despite a strict fasting protocol. The uptakes of ^{68}Ga-NOTA-RGD and ^{18}FDG in atherosclerotic plaque were similar to those in a previous study of [^{18}F]galacto-RGD and ^{3}H-deoxy glucose (DG) using autoradiography, in which the plaque-to-normal vessel ratios were 1.5 for ^{3}H-DG and 1.3 for [^{18}F]galacto-RGD [11]. However, the present study included the thoracic aorta in the VOI without discrimination of the plaque portion, which would result in underestimation of uptake by plaque itself.

The tracer kinetics in humans demonstrates the appropriateness of the reversible binding model and Logan plotting for ^{68}Ga-NOTA-RGD, which can be applied to future studies using tracer kinetic parameters. Additionally, although the number of cases was small and the overall serum hsCRP level was low, our human study demonstrated a tendency of correlation between the uptake of ^{68}Ga-NOTA-RGD and hsCRP, which is the most commonly used serum inflammation marker of atherosclerotic diseases. In a recent study, the mean aorta-to-jugular ratio of ^{18}FDG uptake was about 1.14 and 1.41 in patients with hsCRP levels <2 and ≥ 2 mg/L [25], respectively. These results are not far from those obtained in the present study (aorta-to-jugular ratio up to 1.25).

Atherosclerosis is an inflammatory process, and ^{18}FDG PET, which is used to visualize inflammation non-specifically, is a powerful imaging tool for atherosclerosis. However, molecular imaging methods for more specific processes are required for non-invasive diagnoses, prognostication, and drug-efficacy monitoring. The results of this study showed that ^{68}Ga-NOTA-RGD may be a candidate targeting motif for the molecular imaging of atherosclerosis. However, it is a limitation of this study that uptake of ^{68}Ga-NOTA-RGD was not directly compared with the histopathologic findings for angiogenesis or macrophage accumulation. Additionally, the relatively low image contrast and sensitivity may be a limitation for clinical application of ^{68}Ga-NOTA-RGD PET. Further studies are required to assess the clinical efficacy of ^{68}Ga-NOTA-RGD.

In conclusion, ^{68}Ga-NOTA-RGD demonstrated significant uptake in atherosclerotic aortas in an animal model. In a pilot human study, the appropriateness of the reversible binding model and Logan plotting for tracer kinetic studies was demonstrated. Also, the aorta-to-jugular ratios for human ^{68}Ga-NOTA-RGD PET were comparable to those reported for ^{18}FDG PET. Thus, ^{68}Ga-NOTA-RGD has potential as an in vivo atherosclerosis imaging agent. However, the degree of imaging contrast and sensitivity of ^{68}Ga-NOTA-RGD PET were lower than those of ^{18}FDG PET, which may limit its clinical application.

Acknowledgments This study was supported by a grant of the Korea Healthcare Technology R&D Project, Ministry of Health & Welfare, Republic of Korea (A090633).

References

1. Hackett D, Davies G, Maseri A. Pre-existing coronary stenoses in patients with first myocardial infarction are not necessarily severe. Eur Heart J. 1988;9:1317–23.
2. Murabito JM, Evans JC, Larson MG, Levy D. Prognosis after the onset of coronary heart disease. An investigation of differences in outcome between the sexes according to initial coronary disease presentation. Circulation. 1993;88:2548–55.
3. Sanz J, Fayad ZA. Imaging of atherosclerotic cardiovascular disease. Nature. 2008;451:953–7.
4. Ogawa M, Magata Y, Kato T, Hatano K, Ishino S, Mukai T, et al. Application of 18F-FDG PET for monitoring the therapeutic effect of antiinflammatory drugs on stabilization of vulnerable atherosclerotic plaques. J Nucl Med. 2006;47:1845–50.

5. Tahara N, Kai H, Ishibashi M, Nakaura H, Kaida H, Baba K, et al. Simvastatin attenuates plaque inflammation: evaluation by fluorodeoxyglucose positron emission tomography. J Am Coll Cardiol. 2006;48:1825–31.
6. Arauz A, Hoyos L, Zenteno M, Mendoza R, Alexanderson E. Carotid plaque inflammation detected by 18F-fluorodeoxyglucose-positron emission tomography. Pilot study. Clin Neurol Neurosurg. 2007;109:409–12.
7. Tahara N, Kai H, Yamagishi S, Mizoguchi M, Nakaura H, Ishibashi M, et al. Vascular inflammation evaluated by [18F]-fluorodeoxyglucose positron emission tomography is associated with the metabolic syndrome. J Am Coll Cardiol. 2007;49:1533–9.
8. Potter K, Lenzo N, Eikelboom JW, Arnolda LF, Beer C, Hankey GJ. Effect of long-term homocysteine reduction with B vitamins on arterial wall inflammation assessed by fluorodeoxyglucose positron emission tomography: a randomised double-blind, placebo-controlled trial. Cerebrovasc Dis. 2009;27:259–65.
9. Burtea C, Laurent S, Murariu O, Rattat D, Toubeau G, Verbruggen A, et al. Molecular imaging of alpha v beta3 integrin expression in atherosclerotic plaques with a mimetic of RGD peptide grafted to Gd-DTPA. Cardiovasc Res. 2008;78:148–57.
10. Waldeck J, Hager F, Holtke C, Lanckohr C, von Wallbrunn A, Torsello G, et al. Fluorescence reflectance imaging of macrophage-rich atherosclerotic plaques using an alphavbeta3 integrin-targeted fluorochrome. J Nucl Med. 2008;49:1845–51.
11. Laitinen I, Saraste A, Weidl E, Poethko T, Weber AW, Nekolla SG, et al. Evaluation of alphavbeta3 integrin-targeted positron emission tomography tracer 18F-galacto-RGD for imaging of vascular inflammation in atherosclerotic mice. Circ Cardiovasc Imaging. 2009;2:331–8.
12. Jeong JM, Hong MK, Chang YS, Lee YS, Kim YJ, Cheon GJ, et al. Preparation of a promising angiogenesis PET imaging agent: 68 Ga-labeled c(RGDyK)-isothiocyanatobenzyl-1,4,7-triazacyclononane-1,4,7-triacetic acid and feasibility studies in mice. J Nucl Med. 2008;49:830–6.
13. Zhang X, Xiong Z, Wu Y, Cai W, Tseng JR, Gambhir SS, et al. Quantitative PET imaging of tumor integrin alphavbeta3 expression with 18F-FRGD2. J Nucl Med. 2006;47:113–21.
14. Patsenker E, Popov Y, Stickel F, Schneider V, Ledermann M, Sagesser H, et al. Pharmacological inhibition of integrin alphavbeta3 aggravates experimental liver fibrosis and suppresses hepatic angiogenesis. Hepatology. 2009;50:1501–11.
15. Tahara N, Imaizumi T, Virmani R, Narula J. Clinical feasibility of molecular imaging of plaque inflammation in atherosclerosis. J Nucl Med. 2009;50:331–4.
16. Aziz K, Berger K, Claycombe K, Huang R, Patel R, Abela GS. Noninvasive detection and localization of vulnerable plaque and arterial thrombosis with computed tomography angiography/positron emission tomography. Circulation. 2008;117:2061–70.
17. Tawakol A, Migrino RQ, Bashian GG, Bedri S, Vermylen D, Cury RC, et al. In vivo 18F-fluorodeoxyglucose positron emission tomography imaging provides a noninvasive measure of carotid plaque inflammation in patients. J Am Coll Cardiol. 2006;48:1818–24.
18. Graebe M, Pedersen SF, Borgwardt L, Hojgaard L, Sillesen H, Kjaer A. Molecular pathology in vulnerable carotid plaques: correlation with [18]-fluorodeoxyglucose positron emission tomography (FDG-PET). Eur J Vasc Endovasc Surg. 2009;37:714–21.
19. Wu YW, Kao HL, Chen MF, Lee BC, Tseng WY, Jeng JS, et al. Characterization of plaques using 18F-FDG PET/CT in patients with carotid atherosclerosis and correlation with matrix metalloproteinase-1. J Nucl Med. 2007;48:227–33.
20. Rominger A, Saam T, Wolpers S, Cyran CC, Schmidt M, Foerster S, et al. 18F-FDG PET/CT identifies patients at risk for future vascular events in an otherwise asymptomatic cohort with neoplastic disease. J Nucl Med. 2009;50:1611–20.
21. Jaffer FA, Libby P, Weissleder R. Molecular imaging of cardiovascular disease. Circulation. 2007;116:1052–61.
22. Moulton KS, Vakili K, Zurakowski D, Soliman M, Butterfield C, Sylvin E, et al. Inhibition of plaque neovascularization reduces macrophage accumulation and progression of advanced atherosclerosis. Proc Natl Acad Sci USA. 2003;100:4736–41.
23. Higuchi T, Bengel FM, Seidl S, Watzlowik P, Kessler H, Hegenloh R, et al. Assessment of alphavbeta3 integrin expression after myocardial infarction by positron emission tomography. Cardiovasc Res. 2008;78:395–403.
24. Haukkala J, Laitinen I, Luoto P, Iveson P, Wilson I, Karlsen H, et al. 68Ga-DOTA-RGD peptide: biodistribution and binding into atherosclerotic plaques in mice. Eur J Nucl Med Mol Imaging. 2009;36:2058–67.
25. Yang SJ, Kim S, Choi HY, Kim TN, Yoo HJ, Seo JA, et al. High-sensitivity C-reactive protein in the low- and intermediate-Framingham risk score groups: analysis with (18)F-fluorodeoxyglucose positron emission tomography. Int J Cardiol. 2013;163:277–81.